



SPECTRAL ANALYSIS OF SOURCE PARAMETERS OF THE 1999 KOCAELI AND DÜZCE EARTHQUAKE AFTERSHOCK SEQUENCES

Eser DURUKAL¹, Yeliz ÇATALYÜREKLİ²

SUMMARY

Source parameters of the 1999 Kocaeli and Düzce, Turkey earthquake aftershock sequences are estimated by spectral analysis of acceleration data. Our data set consists of 484 strong motion acceleration records that correspond to 84 events with magnitudes changing between M_L 1.93 and 6.04. The records were obtained between 21 August 1999-29 December 1999, from the permanent and temporary stations in the region. The seismological parameters are from a catalog compiled from the Kandilli Observatory and TUBITAK data. The records are uniformly corrected for distance, free surface and energy partition effects. The effect of whole path diminution is avoided by considering only records obtained within 40km of the hypocenter. We determine seismic moments (M_0), spectral corner frequencies (f_c), source radii (r), stress drops ($\Delta\sigma$), slip (s), radiated energy (E_{rad}) and source duration (T). We obtain these parameters by (1) eye-fitting a straight line to the displacement spectra, and (2) finding the best-fitting theoretical spectra to the acceleration source spectra and compare the two methodologies. We systematically calculate κ , the near surface attenuation factor, and study its dependence on site conditions, distance and magnitude. We correct for site conditions by (1) accounting for the amplification in the low-frequency part of spectrum only, (2) using frequency-dependent site amplification factors. We discuss the differences that we observe in the source parameters introduced by utilization of different techniques for site effects.

INTRODUCTION

On August 17, 1999 a magnitude $M_w=7.4$ earthquake struck the Kocaeli province of Turkey and three months after, on November 12, 1999 the $M_w=7.2$ Düzce earthquake took place to the immediate east of the fault rupture of the Kocaeli earthquake. A large number of aftershocks were recorded by local permanent and temporary accelerometer networks. From them, we choose 84 aftershocks with local magnitudes M_L changing between 1.93 and 6.04 for an analysis of their source parameters by spectral analysis (Brune [1], [2]).

¹ Assoc. Prof., Boğaziçi University, Kandilli Observatory and Earthquake Research Institute, Department of Earthquake Engineering, Istanbul, Turkey, Email: durukal@boun.edu.tr

² M.Sc. Student, Boğaziçi University, Kandilli Observatory and Earthquake Research Institute, Department of Earthquake Engineering, Istanbul, Turkey, Email: yelizcat@yahoo.com

Determination of source parameters by spectral analysis is a widely applied approach used for both weak and strong motion data (Roumelioti et al. [3], Margaris and Hatzidimitriou [4], Chen and Atkinson [5], Huang et al [6] , Jin et al. [7], Bindi et al [8], Eyidoğan and Akinci [9], Margaris and Boore [10] among others) In this study we obtain them by (1) eye-fitting a straight line to the displacement spectra, and by (2) finding the best-fitting theoretical spectra to the acceleration source spectra. We compare and study the results yielded by the two methodologies.

On the other hand the spectra can be corrected for site effects using different approaches. Herein, we choose two such methods: (1) correction for site effects using the relative changes in the low-frequency part of the resulting spectrum following an approach similar to Roumelioti et al [3]; (2) frequency dependent site amplification factors. We use the aftershock data set of the Kocaeli and Düzce earthquakes to look at the effect of these two site correction methods on estimated source parameters.

DATA SELECTION AND PREPARATION

In order to estimate the source parameters of the 17 August 1999 Kocaeli (Mw 7.4) and 12 November 1999 Düzce Earthquake (Mw 7.2) aftershock sequences, all aftershocks recorded by the strong motion stations operated by KOERI (Kandilli Observatory and Earthquake Research Institute of Bogazici University), ITU (Istanbul Technical University), ERD (Earthquake Research Department) and ERI-JAPAN (Earthquake Research Institute of University of Tokyo) in the CD collections of KOERI-Turkey (Özbey [11]) and USGS (United States Geological Survey) (Çelebi et al.[12]) are utilized. The majority of the records were sampled at 200 Hz. Only at a few stations (Derince, Tepetarla, Seka and Sakarya, all aftershock stations of ERD) the sampling rate was 100 Hz. These two sets were subject to data selection by the following criteria: (1) each event in the data set should be recorded by at least four stations to reach a meaningful average (source parameters obtained from these records are averaged to yield the parameters of the event); (2) the hypo-central distances should be less than 40 km to minimize the effect of whole path diminution $Q(f)$. The final data set consists of 494 (x 2 for two horizontal components) acceleration records corresponding to 84 aftershocks recorded between 21 August-29 December 1999. Local magnitudes range from 1.93 to 6.04, while the hypo-central distances are between 5.77 km and 39.89 km.

The seismological parameters that correspond to the recorded aftershocks are compiled from Özalaybey et al. [13], Karabulut et al. [14] and Kalafat et al. [15]. In Kalafat et al. [15] all magnitudes are in duration magnitude, M_D , as is systematically reported by KOERI. They are converted to local magnitude M_L by:

$$M_L = -1.50 + 1.37M_D \quad (1)$$

Equation (1) is computed using the data set provided by Görgün [16].

Figure 1 shows the epicentres of the analysed aftershocks, the mainshocks of Kocaeli and Düzce earthquakes, and the locations of the sixty-four strong motion stations. The breakdown of records with respect to local magnitude, M_L is presented in Figure 2.

Before proceeding with the calculation of the source parameters, each record was baseline corrected, band-pass filtered between 0.3 Hz and 25 Hz and re-sampled at 50 Hz. A time window containing the S-wave was selected and was subject to 10% cosine tapering. The lengths of the selected S-wave windows are shown in Figure 3.

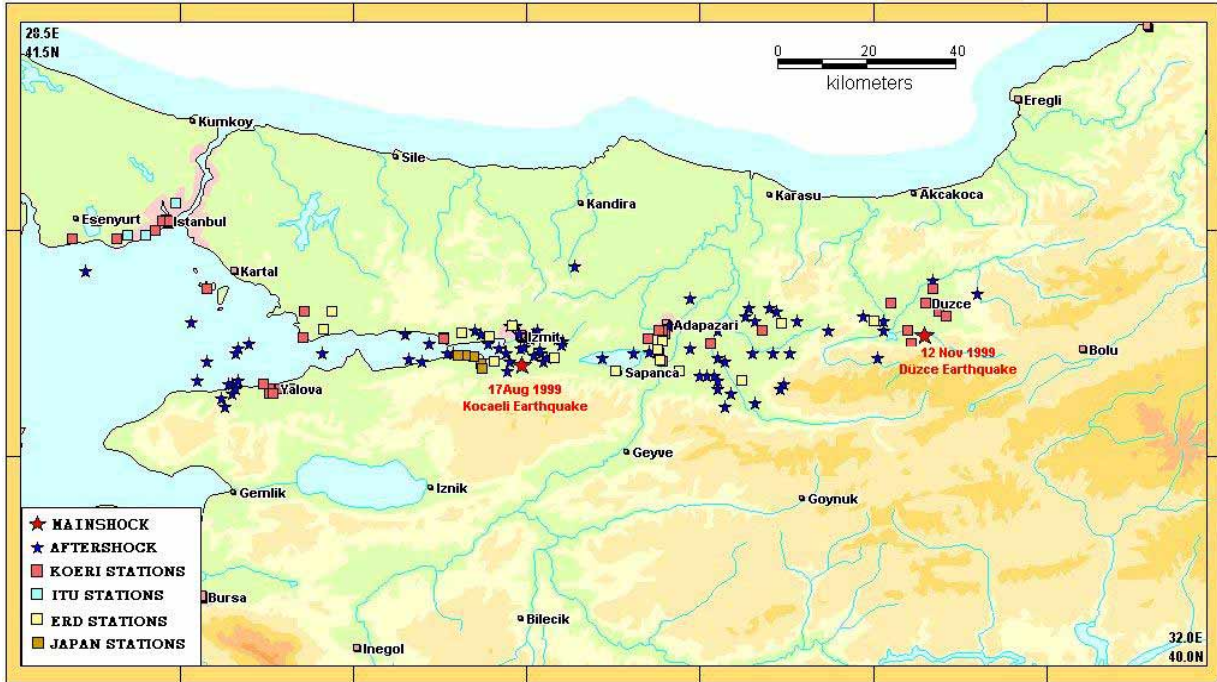


Figure 1. The stations and events

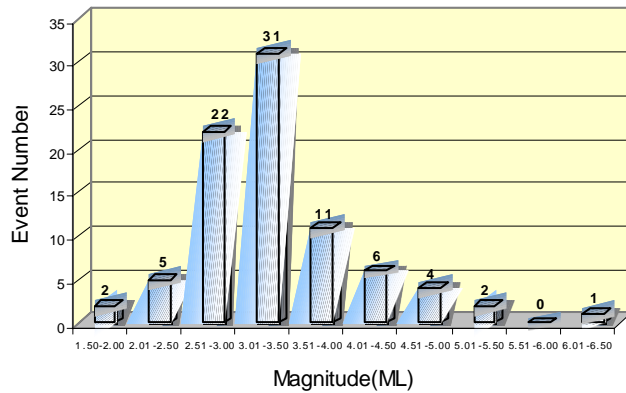


Figure 2. Breakdown of events in the data set with respect to local magnitude M_L .

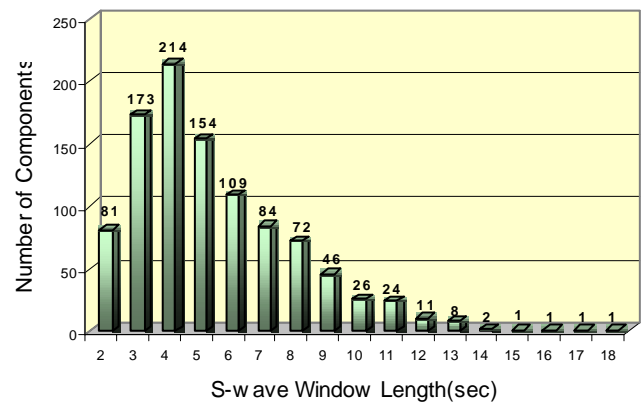


Figure 3. S-wave window lengths used in each component

METHODOLOGY

The radiated spectrum can be expressed by (Boore [17])

$$R(f) = CS(f)D(f)A(f)I(f) \quad (2)$$

where $R(f)$ is the radiated spectrum, C is the scaling factor, $S(f)$ is the source spectrum, $D(f)$ is the diminution factor, $A(f)$ is the site amplification factor, and $I(f) = (2\pi f)^p$ accounts for instrumental response ($p = 1$ or 2 for velocity and acceleration, respectively). The scaling factor C is given by

$$C = (F_s R_{\theta, \varphi} P) / (4\pi \rho \beta^3 R) \quad (3)$$

where F_s is the factor for the free surface effect; $R_{\theta,\phi}$ is the S-wave radiation pattern; P accounts for the partition of energy between the two horizontal components; ρ is the density; β is the average shear-wave velocity around the fault; and R is the hypo-central distance.

The source spectrum, $S(f)$, is represented by Brune's [2] ω^2 model of shear waves for the ground acceleration at the source as

$$S(f) = CM_0 / [1 + (f / f_c)^2] \quad (4)$$

where M_0 is the seismic moment and f_c is the corner frequency of the spectrum. We adopt the method proposed by Andrews [18] for computing the corner frequency, f_c as

$$f_c = \frac{1}{2\pi} \sqrt{\frac{S_{v2}}{S_{d2}}} \quad (5)$$

where S_{v2} and S_{d2} are calculated by the following integrals:

$$S_{d2} = \int_0^{\infty} d^2(f) df \quad (6)$$

$$S_{v2} = \int_0^{\infty} v^2(f) df \quad (7)$$

where $v(f)$ and $d(f)$ are respectively the velocity and the displacement spectra at the source.

$D(f)$ in equation (2) models the attenuation of radiated waves due to geometric spreading and crustal effects and is expressed as:

$$D(f) = \frac{1}{R} \exp\left[\frac{-\pi f R}{\beta Q(f)}\right] \quad (8)$$

where $Q(f)$ is the whole path attenuation factor. Since the hypocentral distances were restricted to 40 km in this work, the displacement spectra were not corrected for the effect of whole path attenuation (Q), since this effect is expected to be negligible at these distances. We only consider the effect of geometrical spreading accounted for by $1/R$.

The effect of local site conditions, $A(f)$ is separated into the effect of high frequency diminution modeled using the kappa (κ) parameter of Anderson and Hough [19] as $\exp(-\pi\kappa f)$ and the effect of site amplification modeled by the amplification functions for NEHRP site classes as provided by Boore and Joyner [20].

The low-frequency level, Ω_0 , of the displacement spectrum is related to seismic moment, M_0 by (Keilis-Borok [21]):

$$M_0 = \frac{4\pi\rho R\beta^3\Omega_0}{F_s R_{\theta,\phi}} \quad (9)$$

The radii of the seismic sources are found from the model of Brune [1], [2] as:

$$r = \frac{0.37\beta}{f_c} \quad (10)$$

where r is the source radius in meters. Corner frequency, f_c , is the average value for each event in the data set. The shear wave velocity β is in km/sec.

Stress drop, $\Delta\sigma$, for each event is estimated using the average values of M_0 and r , from (Keilis-Borok [21]):

$$\Delta\sigma = \frac{7M_0}{16r^3} \quad (11)$$

Average co-seismic slip, s , over the circular fault area is found from:

$$s = \frac{M_0}{\pi r^2 \mu} \quad (12)$$

where μ is the rigidity modulus of the fault material.

Radiated energy, E_{rad} , is found as (Andrews [18]):

$$E_{rad} = 4\pi\rho\beta S_{v2} \quad (13)$$

Maximum slip velocity, v_{max} can be calculated from (Beresnev [22]):

$$v_{max} = (2\pi/e)(M_0/\rho\beta^2 A)fc \quad (14)$$

where e is the base of the natural logarithm and A is the rupture area found from r assuming a circular rupture.

The source duration, T is found using (Beresnev [22]):

$$T \approx 0.6/fc \quad (15)$$

Apparent stress, σ_a is defined by:

$$\sigma_a = \frac{\mu E_{rad}}{M_0} \quad (16)$$

Brune stress drop, σ_B (Brune [1]) is calculated as:

$$\sigma_B = \frac{M_0 fc^3}{(4.910^6 \beta)^3} \quad (17)$$

We calculate source parameters (1) by eye-fitting a straight line to the displacement spectra and (2) by finding the best-fitting theoretical spectra to the acceleration source spectra. In case (1) we find seismic moment from equation (9), f_c from equation (5) and other parameters that are related to the two by equations (10) through (16).

Seismic moments of each event are calculated from means of the logarithms of seismic moments found at different stations, as per Roumelioti et al. [3], by

$$M_0 = \text{anti log} \left\{ \frac{1}{N} \sum_{i=1}^N \log M_{0i} \right\} \quad (18)$$

where N is the number of the components (=number of stations \times 2) in the data set and M_{0i} is the seismic moment determined from (9), for the i^{th} record.

Average values of f_c for each earthquake are determined using the equation:

$$f_c = \text{anti log} \left\{ \frac{1}{N} \sum_{i=1}^N \log f_{ci} \right\} \quad (19)$$

where f_{ci} is the corner frequency for the the i^{th} record computed using equation (5).

As the second approach, we determine the source parameters as those that would produce the best fitting theoretical spectra to the actual one. The theoretical spectra are modeled by equation (2). Effect of whole path attenuation is ignored. Spectral decay parameter, kappa (κ) is calculated for all records and used in modeling of high frequency diminution. Seismic moment is determined from the best-fitting theoretical spectrum. Corner frequency, f_c , is calculated from equation (5). Event averages of M_o and f_c , are calculated using equations (18) and (19) respectively. Other parameters are found by equations (10) through (16).

Constants in the analysis are assumed as follows: $\rho = 2.7 \text{ g/cm}^3$, $\beta = 3.3 \text{ km/ sec}$, $P = 0.71$, $R_{\theta\phi} = 0.63$, $F = 2.0$.

ESTIMATION OF SOURCE SPECTRAL PARAMETERS - COMPARISON OF METHODOLOGIES

We estimate seismic moments by the two approaches as outlined in the previous section. At this stage we neglect the effects of local site conditions and are interested only in knowing how the different approaches applied effect the resultant seismic moments. Methodologies for correcting for site effects have their own differences as well, thus introducing another dimension of uncertainty that we will look at in coming sections. An example for the fitted spectra to the real data is provided in Figure 4.

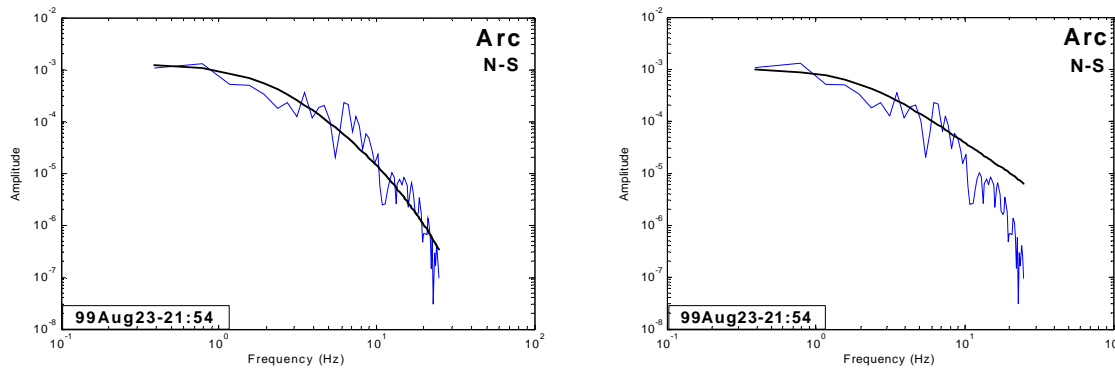


Figure 4. Fit of theoretical displacement spectrum with the recorded spectrum, based on seismic moments estimated by eye-fitting a straight line to the low-frequency part of the displacement spectrum (right) and by finding the best-fitting theoretical spectrum (left)

In Figure 5 we show seismic moments found by eye-fitting a straight line to the low-frequency part of the spectrum, denoted by M_oK , and obtained by best fitting theoretical spectra, called M_o , together. It can be observed that the log values of moments found by the best-fitting spectrum method are systematically higher than the M_oK values by about 1.2. In terms of local magnitude, M_L , this means a difference of 0.5 for the same seismic moment (Figure 6). From Figure 6, a change of trend in M_L vs $\log M_o$ relationship can be observed. This is due to the fact the majority of our data set is from events with local magnitudes between 3 and 3.5. The data should be complemented with more M_o estimations from $M_L > 4$ earthquakes to constrain it better for higher magnitudes.

Figure 7 and figure 8 show the seismic moments plotted against source radius, average slip and stress drop.

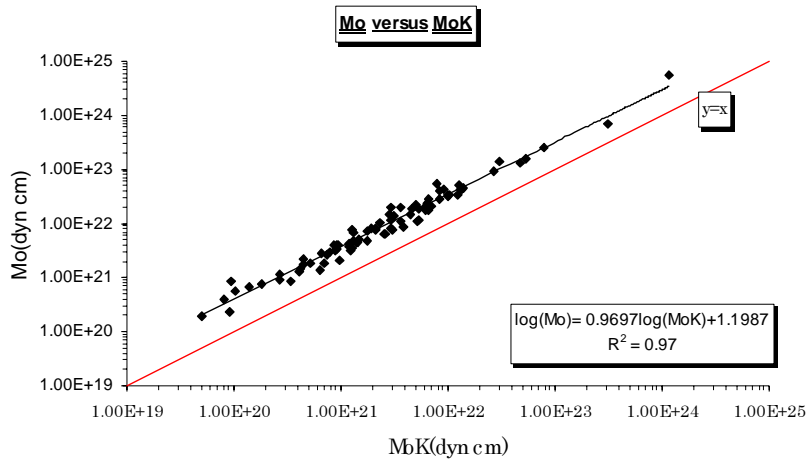


Figure 5. Relation between seismic moments estimated by eye-fitting a straight line to the low-frequency part of the displacement spectrum, M_oK and by finding the best-fitting theoretical spectrum, M_o

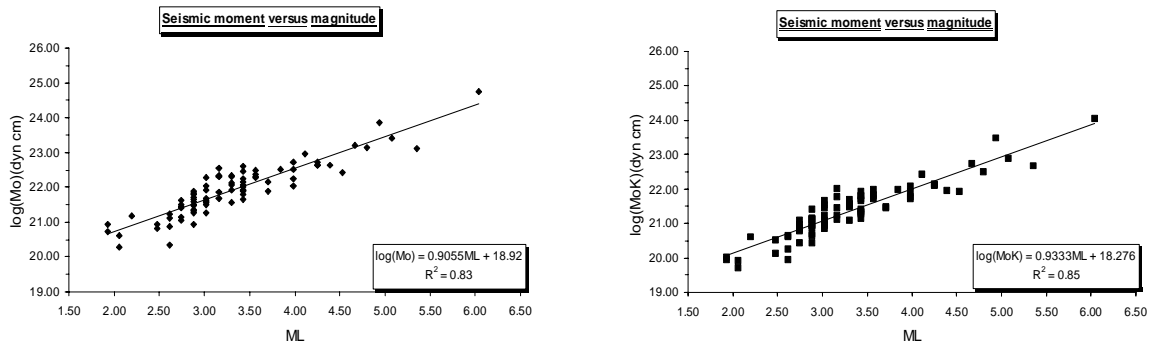


Figure 6. Seismic moment, M_o versus local magnitude M_L . Seismic moments are estimated by eye-fitting a straight line to the low-frequency part of the displacement spectrum (right) and by finding the best-fitting theoretical spectrum (left)

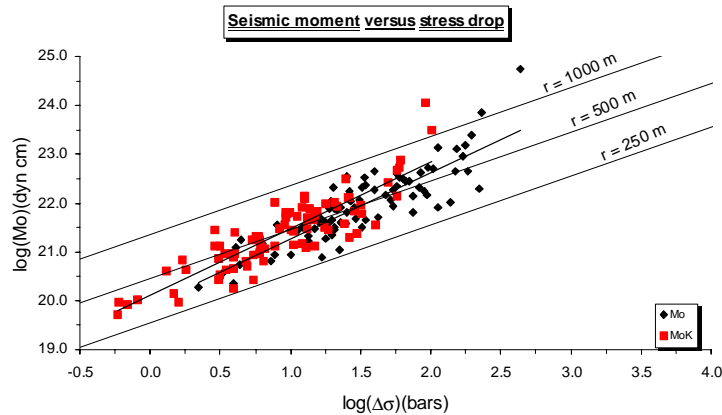


Figure 7. Seismic moment, M_o versus stress drop $\Delta\sigma$. See the caption of Figure 5 for an explanation of M_o and M_oK .

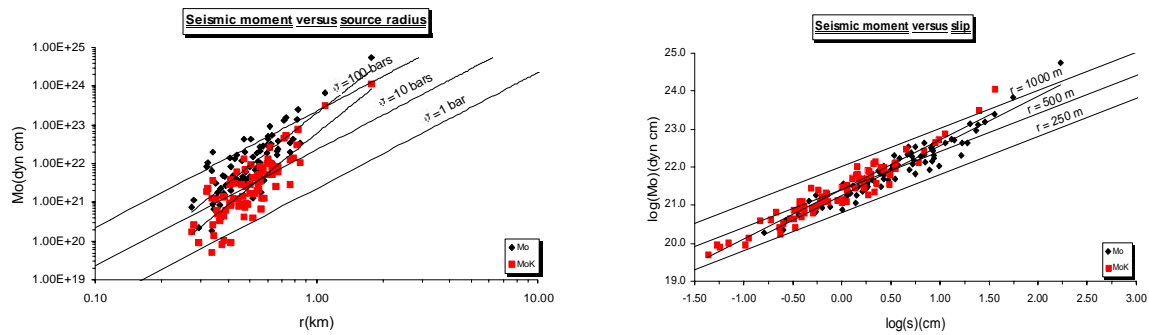


Figure 8. Seismic moment, M_0 versus source radius (left) and average slip (right)

The difference in seismic moment estimations is directly reflected to stress drop, source radius and seismic slip. The majority of stress drops are around 10 bars for low-frequency estimation, and around 40 bars for the best-fitting spectra method.

NEAR SURFACE ATTENUATION FACTOR, kappa

The exponential decay of the S-wave acceleration spectrum at high frequencies is parameterized using the factor, kappa (κ) (Anderson and Hough [19]). Its association with the near surface soil conditions has been portrayed by many starting with the work of Anderson and Hough [19]. Recently Pruvance and Anderson [23] have noted that kappa is affected also by the source and showed its dependence on magnitude. Before proceeding with analysis we have checked how the size of the selected time-window effects kappa. We have compared kappa's estimated using the windowed accelerations with those obtained using the full time series. We have observed that in general similar kappa's are yielded in both cases. Another issue is when to apply the kappa correction to the spectra, i.e. before or after correction for local site effects. This question has been addressed by Margaritis and Boore [10]. They have observed that practically the estimation of kappa is not effected by the order in the calculation steps.

The dependence of the near surface attenuation factor on earthquake magnitude, its association with local site conditions and its variation with distance can be found in Figures 9 through 11. Average kappa values found for each event in our data set have been used in Figure 9. In Figure 10 and 11 we use average kappa of two horizontal components for each record in the data set. The results are for windowed accelerations and have been found before correcting the spectra for site effects.

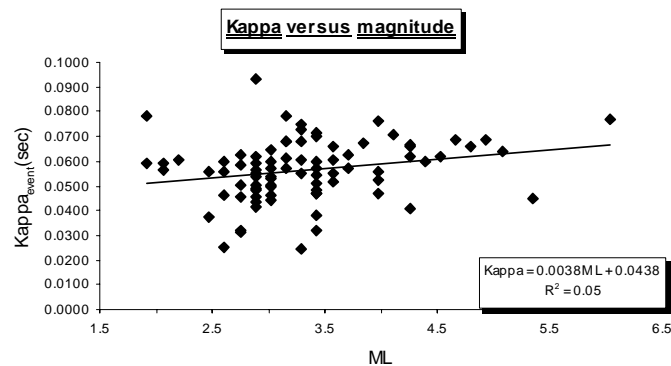


Figure 9. Kappa versus local magnitude

We observe a slight tendency of kappa to increase with magnitude (Figure 9). This is an observation parallel to Purvance and Anderson [23]. Furthermore they note that this dependence changes character with the change of filter limits. Here our data are band-pass-filtered between 0.3Hz-25Hz. Our finding overlaps with the results of Purvance and Anderson [23] presented for a similar frequency range.

In the data set we use data from fifty-eight stations. NEHRP site classes are available for forty-seven of them. For the majority the assignment of the site class is taken from Durukal [24]. Five stations are on NEHRP class C type soil and forty-two stations are on D type soil. We observe practically no change of kappa with distance, when we plot kappa values from all stations versus distance (Figure 10, for stations on NEHRP C-type soil and Figure 11 for stations on NEHRP D-type soils). Although there is a wide scatter in data an average kappa of 0.056 for D type soils and an average kappa of 0.041 for C type soils can be found as a result of our analysis.

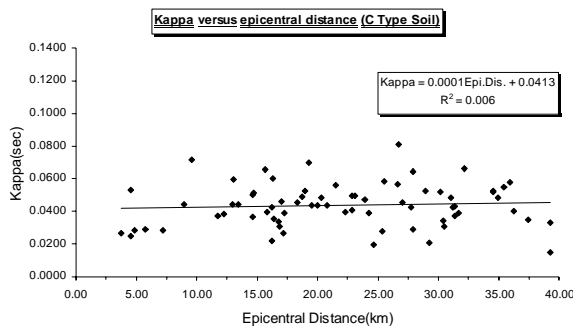


Figure 10. Kappa versus epicentral distance

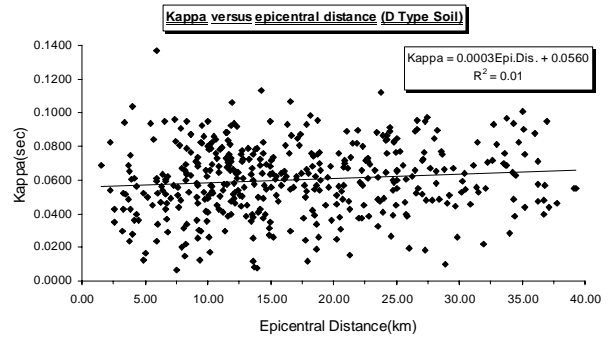


Figure 11. Kappa versus epicentral distance (for stations on NEHRP D-Type Soil)

ACCOUNTING FOR SITE EFFECTS

Quantification of Site Effects at the Stations

For a quantification of the local site effects we turn to the horizontal-to-vertical (H/V) spectral ratio technique of Nakamura [25]. It is considered as a good indicator of amplification of horizontal ground motions due to local soil conditions in the general sense. Chen and Atkinson [5] observe that the H/V ratio is a stable site parameter when averaged over many events at a site, although large variability exists from event to event. When H/V ratios are regionally averaged for all stations of the same site class, they display the overall characteristics corresponding to the site type.

The H/V ratio is calculated as a function of frequency from the Fourier spectra by:

$$(H/V)(f) = \sqrt{H_1(f)H_2(f)} / V(f) \quad (20)$$

where H_1 and H_2 represent the two horizontal components and V is the vertical component.

Before proceeding with the H/V estimations, the signal-to-noise ratios are calculated for all records at these stations and those with signal-to-noise ratios smaller than 3 are left out. The S-wave windows, tapered using a 10% cosine taper, are used for the H/V calculation. The Fourier amplitude spectra of horizontal and vertical components are smoothed to provide a reliable estimate of H/V. In some stations

there are hundreds of records virtually suitable for H/V calculation. It was decided to limit the number of records to be used from one station to 50. Average H/V ratios are found for each strong motion station using all records available at that station (i.e. the records are not limited to the ones that we include in the data set for source spectral analysis).

In Figure 12 we show average H/V ratios for all NEHRP site class C and D stations. In both cases we also indicate the ensemble average of the H/V ratios, which can be considered as the regional H/V ratio for the corresponding site class. It can be observed that the sites on D-type soil show slightly higher H/V amplitudes than the sites on C-type soil; the dominant frequency of the H/V ratio shifts toward lower values with increasing softness of the site conditions (e.g., from C-type to D-type soil in our case). It is clear that the effect of different site conditions has to be accounted for in the estimation of source spectral parameters, which is done in the next section.

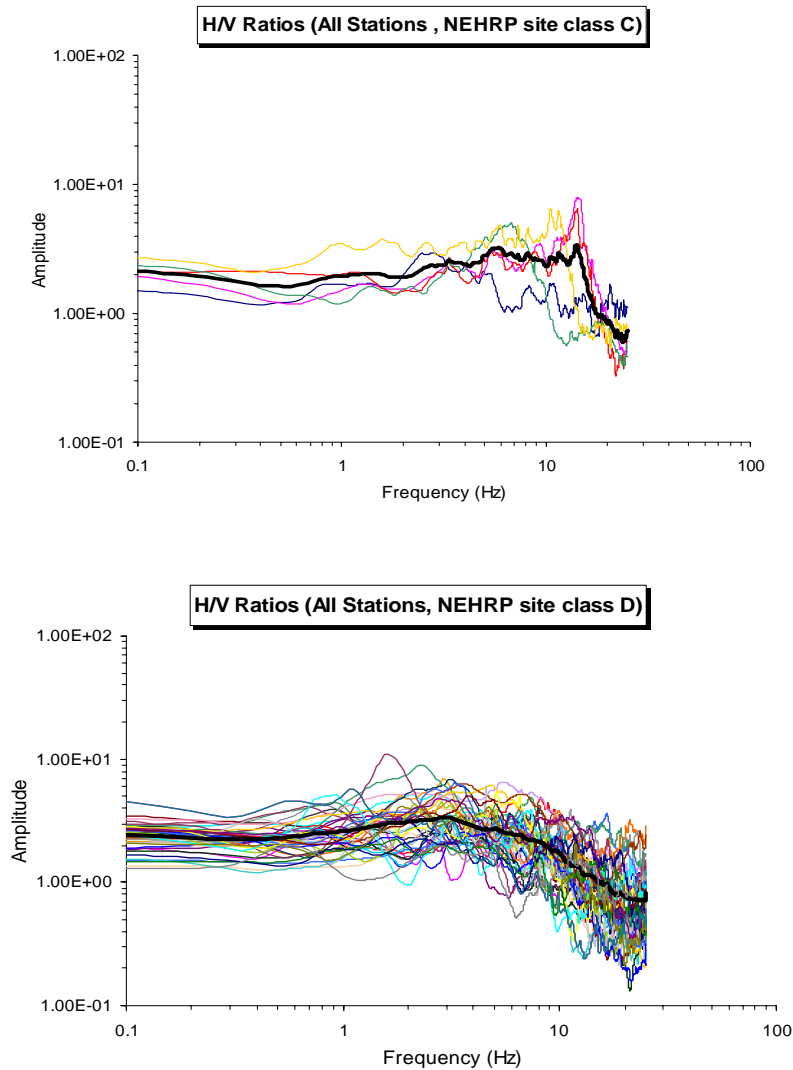


Figure 12. Average H/V ratios for NEHRP site class C type stations (top) and NEHRP site class D type stations (bottom)

Accounting For Site Effects In The Low-Frequency Range

We choose to correct for site conditions (1) by accounting for the amplification in the low-frequency part of spectrum only, and (2) by using the frequency-dependent site amplification factors proposed for Boore and Joyner [20].

Roumelioti et al. [3] outline a procedure to account for the overestimation of the seismic moment due to site amplification in the low-frequency part of the spectrum. This procedure is applied to the aftershock data set of the Kocaeli and Düzce earthquakes. Roumelioti et al. [3] showed the systematic dependence of estimated M_0 values on site conditions and noted that, when plotted, the data can be described by a general equation of the form:

$$\log M_0 = aM_L + b_{station} \quad (21)$$

The slope, a , of the least squares' fit was almost equal to 1, while parameter b showed a variation from station to station. Assuming a fixed slope $a=1$, the values of the parameter b were recalculated and a mean $b_{station}$ was found for each site. The station with the minimum value of the $b_{station}$ is determined. It was observed that this station was on a firm site. The initial values of $\log(M_0)$ were reduced by $(b_{station}-b_{sta.min.})$. The values of $\log(M_0)$ before the correction for site effect for the station 1409 are plotted in Figure 13, together with the reduced values accounting for the amplification of the low-frequency part of the spectrum.

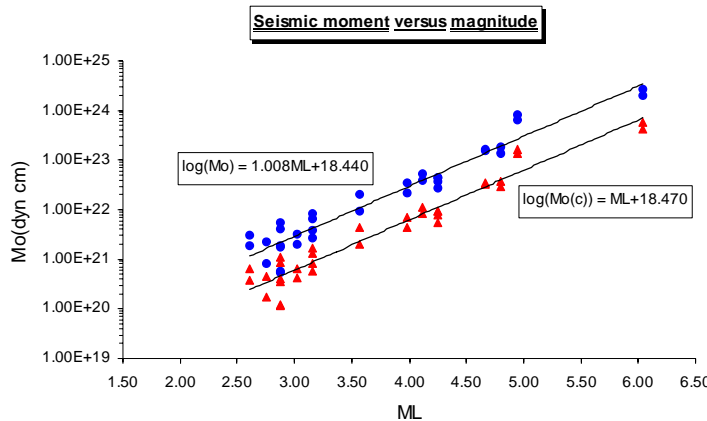


Figure 13. Seismic moment versus magnitude for station 1409 (Serdivan) before (shown in blue) and after (shown in red) site correction.

For the fifty-eight stations that we consider in our data set we have plotted the $\log(M_0)$ versus M_L curves and performed a least squares line fitting. We have observed that the majority of the slopes are in the vicinity of 1. The general range of slopes was between 0.75-1.25. There were a couple of stations with slopes falling outside this range the data from which were removed. There are only NEHRP site class C and D type stations in our data set. Ideally this correction should be performed with respect to a rock type station. Yet we have decided to perform this analysis to see whether this type of correction would yield any difference in the results even if it is carried out with respect to a site class C station. In our data set the station with the minimum b value is station Arçelik (ARC). Initial values of $\log(M_0)$ obtained in each station are reduced by the difference $b_{station}-b_{Arc}$. The relationships between several source parameters found by taking into account the site correction are plotted in Figure 13.

Correction For Site Effects Using Boore and Joyner [20] Type Site Amplification Factors

Boore and Joyner [20] have proposed frequency dependent site amplification values specific to NEHRP site classes to be used in strong motion simulation and for spectral studies. Our stations are classified as NEHRP site class C or D. There are no rock stations in our data set. The stations with no assigned NEHRP site class are assumed to be on generic soil. We use the frequency dependent site amplification functions as provided by Boore and Joyner [20] for C-type, D-type and generic soil in the analysis. They are corrected for near surface attenuation ($e^{-\pi\kappa f}$) using the κ (kappa) value for each record in each run. After reducing the site effects by this approach, seismic moments, corner frequencies and related parameters are found. The results obtained after use of frequency dependent amplification factors are presented in Figure 13.

Results

The site correction carried out has introduced a certain amount of scatter to the resulting source parameters and in general shifted our estimations towards lower values. This can be observed by comparison of Figure 12 with Figures 7 and 8. The majority of stress drops now cluster around 20 bars for Boore and Joyner [20] correction and around 6 bars for correction considering the low-frequency part of spectrum only. Seismic moments estimated after site correction using frequency dependent amplification functions are larger than the ones obtained using the approach correcting only for the site effect on the low-frequency part of spectrum. This is reflected in all sub-figures of Figure 12. A slight decrease in the seismic moment estimation is noted when one compares the results from with and without correction for site effects (i.e. MoK -MoC1 and Mo- MoC2 from Figures 7, 8 and Figure 12). However the effect of scatter introduced by site correction is much more pronounced. Assessed source radii vary between 200 and 1000m, the stress drops change between 1 and 100 bars, source durations are between 0.1s and 0.9 s, corner frequencies vary between 0.8Hz ad 8.0Hz, regardless of the method for site correction.

CONCLUSIONS

S-wave spectral analysis is applied to a set of aftershock data compiled from the strong motion recordings of the Kocaeli and Düzce earthquakes. All records that have been recorded within 40km of the hypocenter are included. We have chosen only those events that have been recorded by at least four stations to reach a meaningful average in obtaining the source parameters. The data set consists of 484 two component strong motion acceleration records that correspond to 84 events with magnitudes changing between M_L 1.93 and 6.04.

We have obtained the source parameters by (1) eye-fitting a straight line to the displacement spectra, and (2) by finding the best-fitting theoretical spectra to the acceleration source spectra. It is observed that method (2) systematically yields higher seismic moments as compared to method (1). This is reflected into other relationships between different source parameters. For example the majority of stress drops found around 10 bars using method (2) and around 40 bars using method (2).

We systematically calculate κ , the near surface attenuation factor, and study its dependence on site conditions, distance and magnitude. An average kappa of 0.056 for D type soils and an average kappa of 0.041 for C type soils can be found. Kappa practically do not vary with distance. It tends to increase however with earthquake magnitude, which implies that kappa is effected by the source as well in addition to local site conditions.

We have obtained average H/V ratios for all the stations in our data set, for which the soil type is known and calculated an average H/V ratio for NEHRP-C type soil stations and NEHRP-D type soil station. In

terms of amplification levels the two curves are similar. In terms of frequency behaviour, the average H/V ratio corresponding to C-type soil has larger high frequency content, as expected.

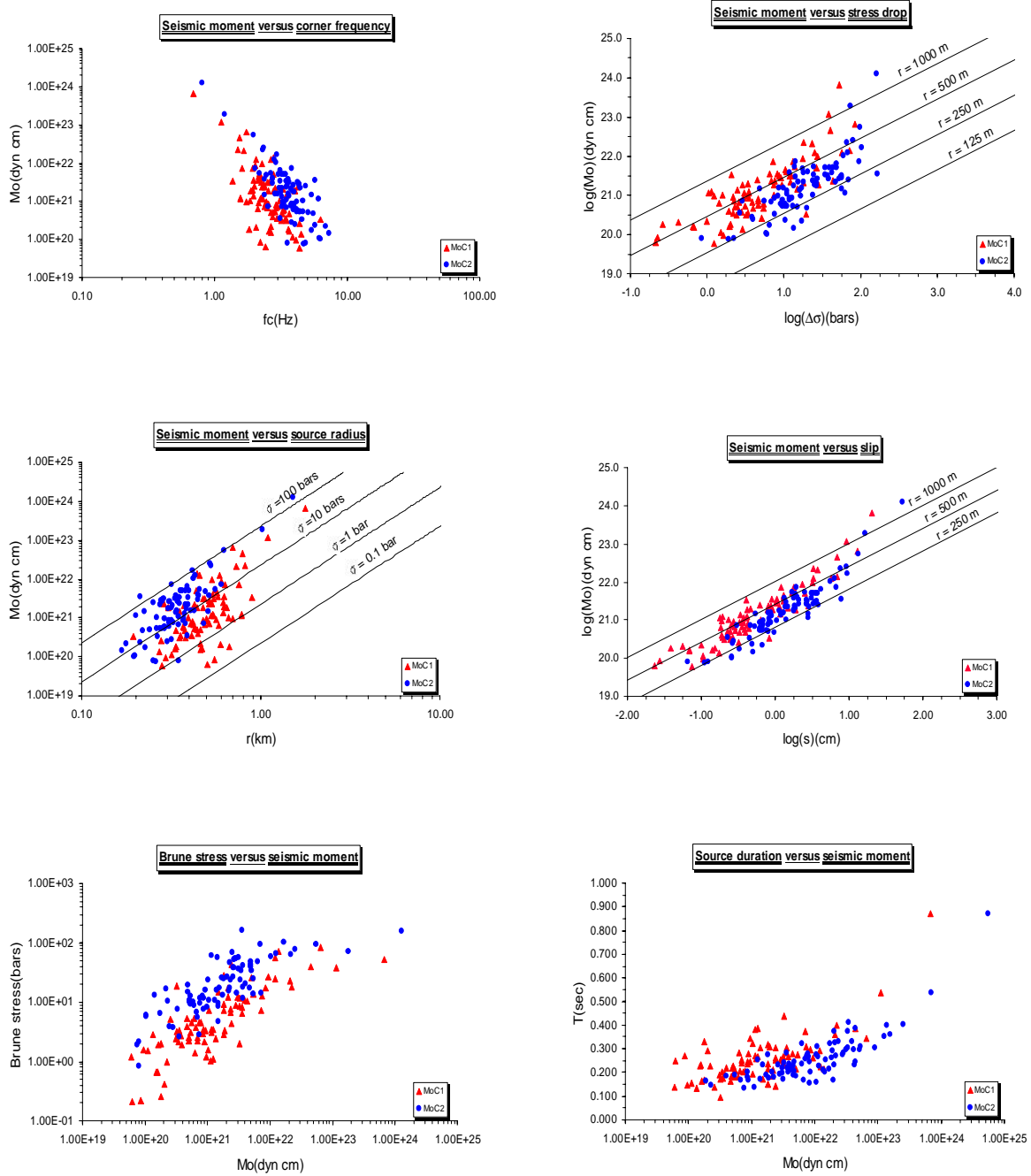


Figure 12. Source parameters estimated by (1) accounting for the amplification in the low-frequency part of spectrum only as proposed by Roumelioti et al [3], shown as MoC1 in red, and (2) using the frequency-dependent site amplification factors proposed for Boore and Joyner [20], indicated as MoC2 in blue.

We correct for site conditions by (1) accounting for the amplification in the low-frequency part of spectrum only as proposed by Roumelioti et al. [3] and (2) using the frequency-dependent site amplification factors proposed for Boore and Joyner [20]. In general the site correction carried out has introduced a certain amount of scatter to the resulting source parameters and shifted our estimations towards lower values. The majority of stress drops now cluster around 20 bars for type (2) correction and around 6 bars for type (1).

A comparison of our results with studies carried out in similar tectonic environments is necessary. A compilation of estimations from previous studies to be reinterpreted with the addition of our data and a uniform source spectral analysis of strong motion data from Turkey are desirable.

REFERENCES

1. Brune JN. "Tectonic stress and the spectra of seismic shear waves from earthquakes". *Journal of Geophysical Research* 1970; 75(26): 4997-5009.
2. Brune JN. "Correction". *Journal of Geophysical Research* 1971; 76: 5002.
3. Roumelioti Z, Kiratzi A, Theodulidis N, Papaioannou C. "S-wave spectral analysis of the 1995 Kozani-Grevena (NW Greece) aftershock sequence". *Journal of Seismology* 2002; 6: 219-236.
4. Margaris BN, Hatzidimitriou PM. "Source spectral scaling and stress release estimates using strong-motion records in Greece". *Bulletin of the Seismological Society of America* 2002; 92(3): 1040-1059.
5. Chen S, Atkinson GM. "Global comparisons of earthquake source spectra". *Bulletin of the Seismological Society of America* 2002; 92(3): 885-895.
6. Huang M-W, Wang J-H, Hwang R-D, Chen K-C. "Estimates of source parameters of two large aftershocks of the 1999 Chi-Chi, Taiwan, earthquake in the Chia-Yi area". *TAO* 2002; 13(3): 299-312.
7. Jin A, Moya CA, Ando M. "Simultaneous Determination of Site Responses and Source Parameters of Small Earthquakes along the Atotsugawa Fault Zone, Central Japan". *Bulletin of the Seismological Society of America* 2000; 90(6): 1430-1445.
8. Bindi D, Spallarossa D, Augliera P, Cattaneo M. "Source parameters estimated from the aftershocks of the 1997 Umbria-Marche (Italy) seismic sequence". *Bulletin of the Seismological Society of America* 2001; 91(3): 448-445.
9. Eyidoğan H, Akinci A. "Site Attenuation and source parameters on the North Anatolian Fault zone, eastern Turkey estimated from the aftershocks of 13 March 1992 Erzincan earthquake". *Journal of Seismology* 1999; 3:363-373.
10. Margaris BN, Boore DM. "Determination of $\Delta\sigma$ and κ_0 from response spectra of large earthquakes in Greece". *Bulletin of the Seismological Society of America* 1998; 88(4): 170-182.

11. Özbey C. “Strong motion data base for the August 17, 1999 Kocaeli earthquake and aftershocks”. CD-Rom. Istanbul: Boğaziçi University, 2000.
12. Çelebi M, Akkar S, Gülerce Ü, Sanlı A, Bundock H, Salkın A. “Main shock and aftershock records of the 1999 Izmit and Düzce, Turkey earthquakes”. Open-File Report 01-163, USGS, 2001.
13. Özalaybey S., Ergin M, Aktar M, Tapırdamaz C, Biçmen F, Yörük A. “The 1999 İzmit aequence in Turkey: seismological and tectonic aspects”. Bulletin of the Seismological Society of America 2002; 92(1): 376-386.
14. Karabulut H, Bouin M-P, Bouchon M, Dietrich M, Cornou C, Aktar M. “The Seismicity in the eastern Marmara sea after the 17 august 1999 İzmit earthquake”. Bulletin of the Seismological Society of America 2002; 92(1): 387-393.
15. Kalafat D, Öz G, Özel N, Kara M et al. “August 17 İzmit, november 12 Düzce earthquakes and aftershock activities”. Istanbul: Boğaziçi University, Kandilli Observatory and Earthquake Research Institute, 2001.
16. Görgün E. “Calibration of various magnitude scales in Turkey using broadband data”. MSc. Thesis. Istanbul: Boğaziçi University, 2003.
17. Boore DM. “SMSIM-fortran programs for simulating ground motions from earthquakes: version 1.0”. Open File Report 96-80-A, USGS, 1996.
18. Andrews DJ. “Objective determination of source parameters and simlarity of earthquakes of different size”. Das S, Boatwright J, Scholz SH, Editors. Earthquake source mechanics. Washington DC: Maurice Ewing Series 6, AGU, 1986: 259-267.
19. Anderson JG, Hough SE. “A model for the shape of the Fourier amplitude spectrum of acceleration at high frequencies”. Bulletin of the Seismological Society of America 1984; 74(5): 1969-1993.
20. Boore DM, Joyner WB. “Site amplifications for generic rock sites”. Bulletin of the Seismological Society of America 1997; 87(2): 327-341.
21. Keilis-Borok V. “On the estimation of the displacement in an earthquake source and of source dimensions”. Annali di Geofisica 1959; 12: 205-214.
22. Beresnev IA. “Source parameters observable from the corner frequency of earthquake spectra”. Bulletin of the Seismological Society of America 2002; 92(5): 2047-2048.
23. Purvance MD, Anderson JG. “A comprehensive study of the observed spectral decay in strong-motion accelerations recorded in Guerrero, Mexico”. Bulletin of the Seismological Society of America 2003; 93(2):600-611.
24. Durukal E. “Critical evaluation of strong motion data for Kocaeli and Düzce (Turkey) earthquakes”. Sol Dynamics and Earthquake Engineering 2002. 22: 589-609.
25. Nakamura Y. “A method for dynamic characteristics estimation of subsurface using microtremors on the ground surface”. QR of RTRI 1989; 30: 25-33.